Supporting Information

Harnessing infrared radiation using carbon dots: photovoltaic devices achieving extraordinary efficiency under faint lighting

*Karan Surana[a], Bhaskar Bhattacharya[b] and Saurabh S. Soni[a,c]**

[a]Department of Chemistry, Sardar Patel University, Vallabh Vidyanagar 388120, Gujarat, India

[b]Department of Physics, Mahila Mahavidyalaya, Banaras Hindu University, Varanasi 221005, Uttar Pradesh, India

[c]Department of Applied and Interdisciplinary Sciences (IICISST), Sardar Patel University, Vallabh Vidyanagar 388120, Gujarat, India

*Corresponding Author: soni_b21@yahoo.co.in, saurabh_soni@spuvvn.edu (SSS)

Materials and Methods

Collard Green leaves were procured from the local market, washed thoroughly with running water and stored in refrigerator. Prior to chopping, the leaves were pressed between tissue papers for eliminating the extra moisture. The leaves were divided into three parts and subjected to different treatments.

(a) The cut leaves were mixed with 50 mL of water and ethanol (equal ratio) and heated at ~ 50 °C for few hours to obtain the extract. The extract was filtered and 30 mL was stored separately as stock solution (CG-WE). The remaining 20 mL was diluted with 40 mL of water and ethanol and subjected to hydrothermal treatment @ 180 °C ± 3 for 8 h. The obtained CD were named as CG.

(b) The cut leaves were submerged in 40 mL DMF for 30 min and the obtained solution was filtered and stored as stock solution (CG-DMF). Half of the solution was diluted with 40 mL DMF and subjected to solvothermal treatment @ 200 °C for 12 h. The obtained CD were tagged as CG-SOV.

(c) The cut leaves were immersed in acetone for 30 min and the obtained solution was filtered and stored as stock solution (CG-ACE). Half of the solution was subjected to microwave treatment @

560 W for 10 min under continuous reflux. The obtained sticky material was mixed with acetone and sonicated for 10 min to obtain the CD termed as CG-MW.

The filtration process was kept the same for all the CD. The treated solutions were first filtered with 0.45 µm Millipore filter followed by 0.20 µm Nexflo syringe filter and stored in dark at room temperature for further use.

For the treatment of TiO_2 electrode with $TiCl_4$ solution the following protocol was followed [a,b]: A beaker was kept in refrigerator with 30 mL of distilled water for over 30 min to achieve a temperature of ~ 5 °C. A pipette was used to add 0.09 M of $TiCl_4$ and the beaker was kept undisturbed in the refrigerator for another 30 min. After bringing the solution to room temperature, the beaker was transferred to a hot-air oven at 70 °C in which the TiO_2 coated electrode was dipped for 30 min. The sintering of the TiO_2 electrode was performed at a slow ramp speed of ~ 4 °C per min.

The polymer electrolyte was a mixture of PEO and PEG (40:60) with 10 – 20 % LiI and 1% I_2 in 20 mL acetonitrile along with 0.5 M of 4-tert butylpyridine.

For the preparation of a 5 x 1 device (CS1.5), double scotch tapes were adhered onto the FTO glasses and the dimensions were cut according to the design as shown in Fig. S1. The FTO coating was retained on the grey shaded portions while etching was performed on rest of the surface. Zn dust was spread carefully on the exposed surface followed by addition of few drops of dilute HCl. The etching was allowed to continue for few minutes following which the FTO washing protocol and rest of the coating process was initiated.

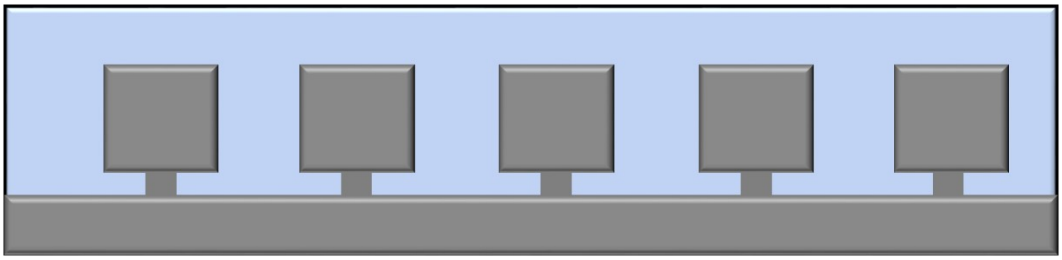

Fig. S1: A Schematic representation of the etched (blue) and FTO retained (grey) regions of the glass substrate.

Characterization tools

The TEM images were obtained using JEOL JEM 2100F field emission gun TEM at an operating voltage of 200 kV. The samples were sonicated thoroughly and placed on Carbon coated Cu grids couple of hours prior to imaging. The absorption study was carried out with Shimadzu 1800 UV-Vis spectrophotometer in the range 700 – 200 nm. The measurement was undertaken by adding 3 mL of the solvent in a quartz cuvette with 40 µL of the solution. The PL measurements were carried out in Horiba FluoroMax-4 spectrometer at various excitation wavelengths. The excitation and emission slit widths were fixed at 5 mm. The quantity taken for measurement was same as the UV-Vis absorption. The lifetime measurement was achieved with Horiba's DeltaFlex time correlated single photon counting (TCSPC) system having an HPPD detector. The fluorescence decays were fitted to bi-exponential fitting for proper analysis. Horiba SZ100 Z was used for analyzing the particle size distribution of the CD by dynamic light scattering (DLS) method and their zeta potential. For this 500 µL of each CD were diluted in 3 mL of water. The I-V characteristics of the devices were evaluated using CHI 660E electrochemical workstation and irradiated with a solar simulator (PET, USA #SS80AAA). Measures were taken to ensure that the photovoltaic characterizations were performed at ~ 25 °C, unless otherwise stated. The incident photon-to-current conversion efficiency (IPCE) measurement of the devices were performed in a dark room using Oriel IQE-200, Newport, USA Quantum Efficiency measurement setup having a 250 W quartz tungsten halogen lamp.

PL Emission

The emission characteristics of CG-WE was taken at 329 nm (absorption maxima). The emission spectra at the other two excitation wavelengths (244 nm and 267 nm) were mostly noisy. Fig. S2a shows that the emission λ_{max} (wavelength maximum) of CG-WE was obtained at 432 nm. The unevenness in the PL emission signifies the wide distribution of particles in the dye. The corresponding carbon dot (CG) shows sharp emission peaks upon excitation at 350 nm (Fig. S2b). The emission intensity of CG gradually increases with increasing excitation wavelengths from 300 nm to 350 nm following which a gradual decrease is observed. The emission λ_{max} is independent of the excitation wavelength up to 350 nm after which it shows excitation dependent behavior, which is a typical nature of most carbon dots [c].

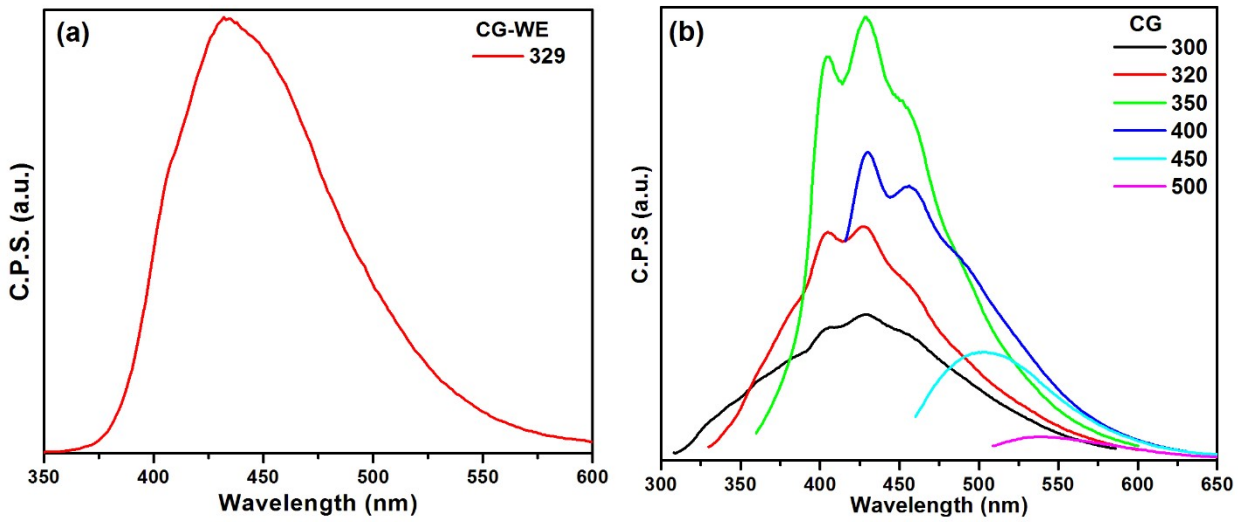

Fig. S2: PL emission of (a) CG-WE and (b) CG

The emission characteristics of CG-DMF dye shows excitation-independent emission behavior [d] with a λ_{max} at 670 nm, which is a typical emission characteristic of chlorophyll a (Fig. S3a) [e]. The emission intensity rises from 350 nm to 430 nm followed by a decline (absorption maxima was at ~ 430 nm). The presence of other pigments led to a low-intensity excitation-dependent emission between 350 nm to 500 nm (Inset Fig. S3a). Similar behavior is noticed in CG-SOV where a red-shift in the emission λ_{max} and a decrease in intensity can be seen with increasing excitation wavelength (Fig. S3b). The emission λ_{max} varies from 427 nm to 528 nm. Small shoulder peaks are also visible beyond 600 nm, which signifies the possibility of a weak red emission. Since, the TEM image confirmed narrow particle size distribution, the excitation-dependent emission would be attributed to the presence of various surface states.

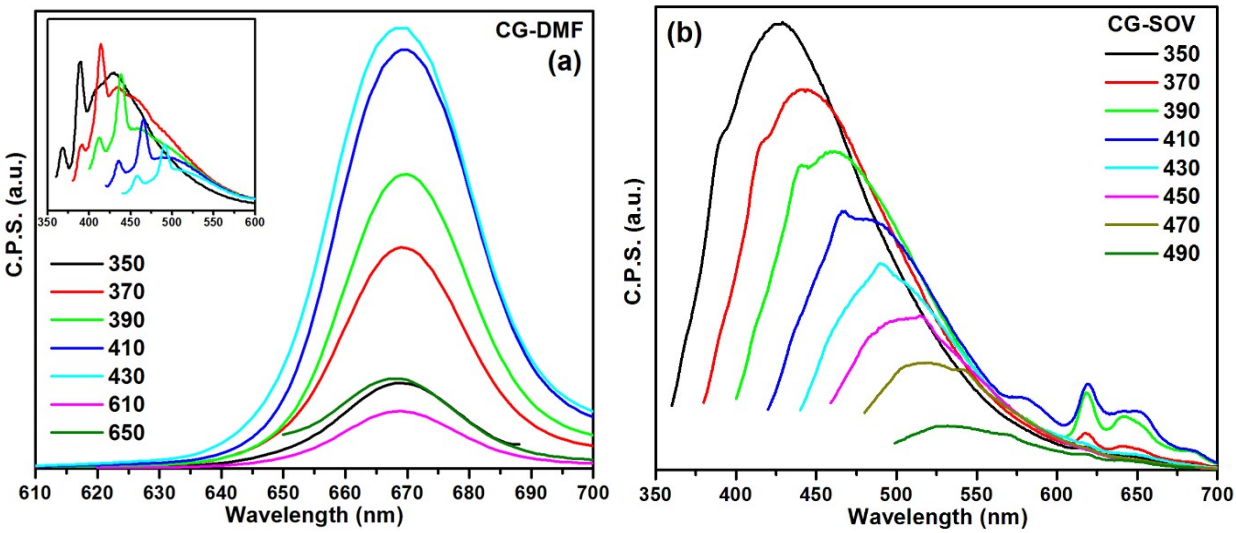

Fig. S3: PL emission of (a) CG-DMF. (Inset) PL between 350 to 600 nm and (b) CG-SOV.

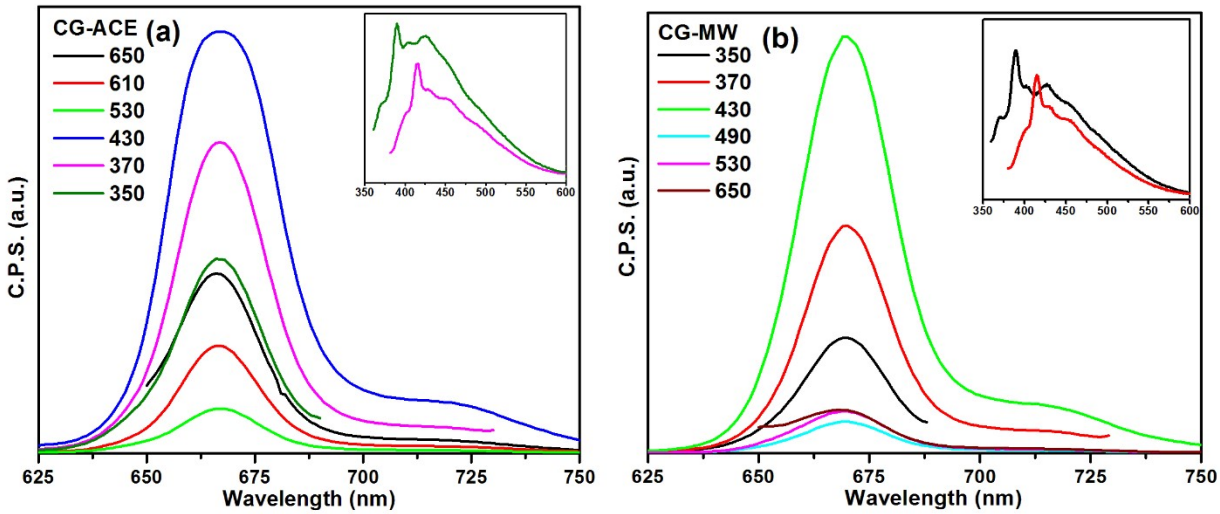

Fig. S4: PL emission of (a) CG-ACE. (Inset) PL between 350 to 600 nm and (b) CG-MW. (Inset) PL between 350 to 600 nm

CG-ACE shows a consistent emission peaks at 670 nm (Fig. S4a), owing to the dominance of chlorophyll a. Also, the emission intensity rises till an excitation wavelength of 430 nm following which it declines, which is an expected behavior. A shoulder peak can be seen between 700 nm to 750 nm, which is also consistent with the fluorescence characteristics of chlorophyll a. Similar emission characteristics are observed in CG-MW (Fig. S4b) with the emission peaks being rather sharp as compared to its dye counterpart.

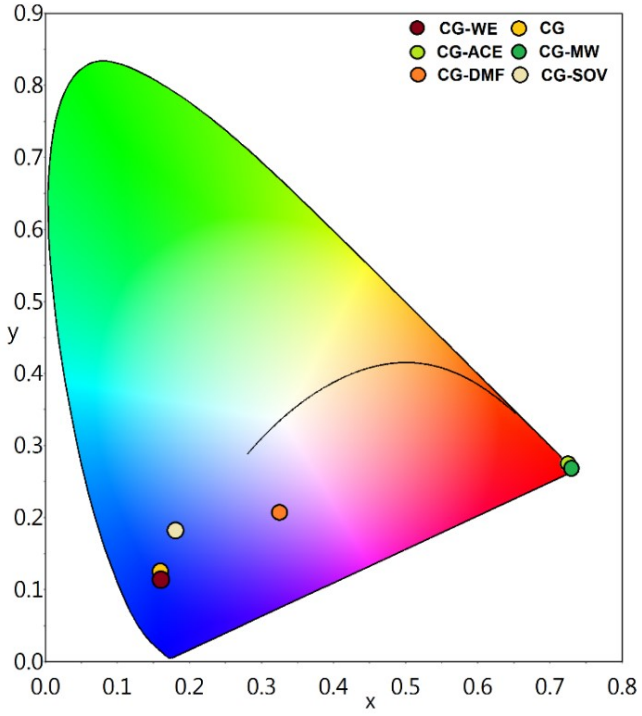

Fig. S5: CIE color coordinates of the dye and their corresponding CD. (The color in the circles were added separately)

The CIE color coordinates of the dyes and their corresponding CD were identified from the PL data using Osram Color Calculator (Fig. S5). As observed in Fig. 1, the luminescence of CG-SOV is quite different from its dye (CG-DMF); the same is reflected in the color coordinates. The rest two dyes and their CD have an almost overlapping nature due to similar luminescence. The obtained coordinates are tabulated in Table T1.

Table T1: CIE color coordinates values of the dyes and their corresponding CD

CD	**CG-WE**	**CG**	**CG-ACE**	**CG-MW**	**CG-DMF**	**CG-SOV**
x, y	0.159, 0.117	0.159, 0.125	0.724, 0.275	0.727, 0.272	0.324, 0.206	0.181, 0.182

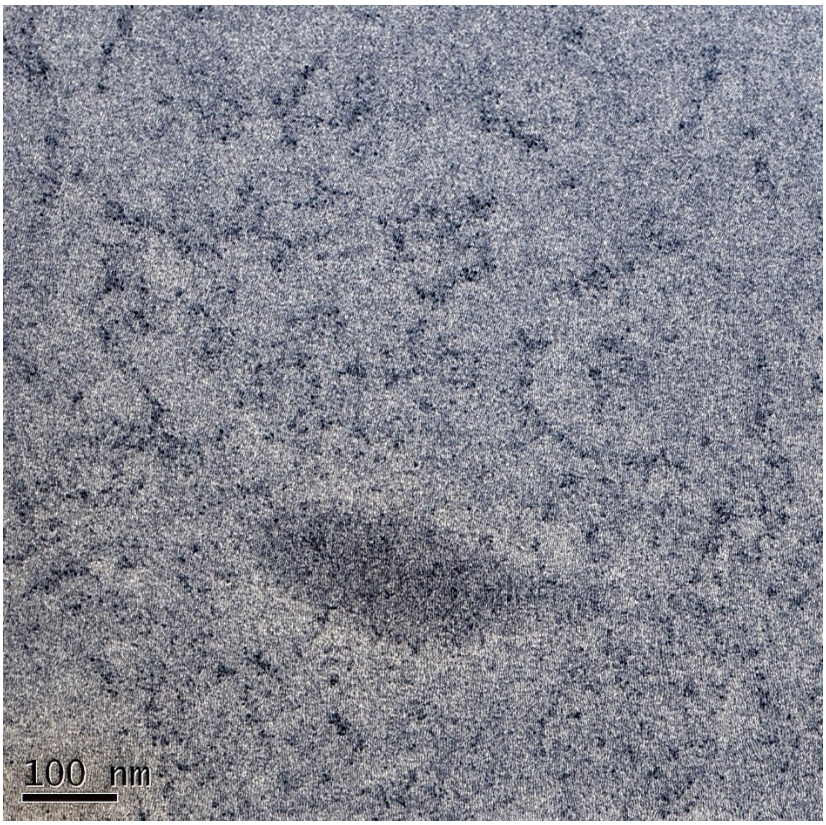

Fig. S6: TEM image of CG. Image quality enhanced online.

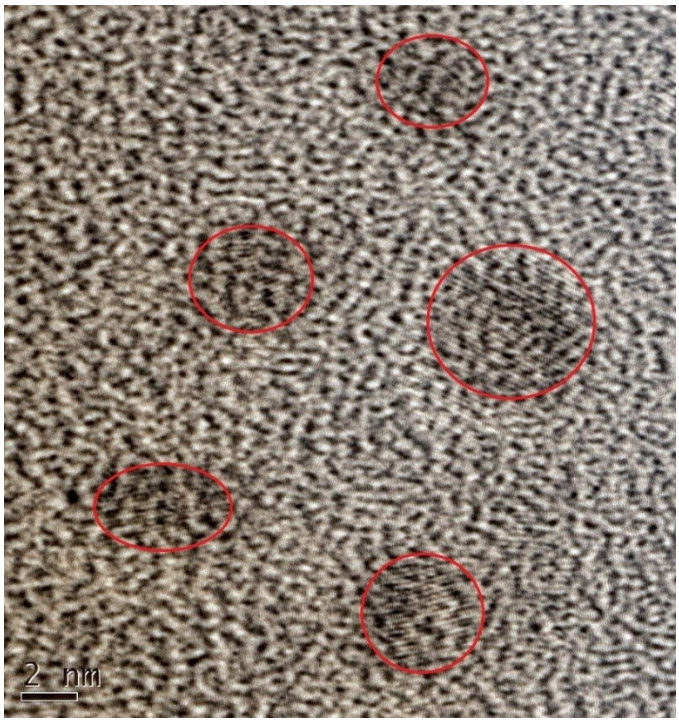

Fig. S7: HRTEM image of CG-SOV with marked particles

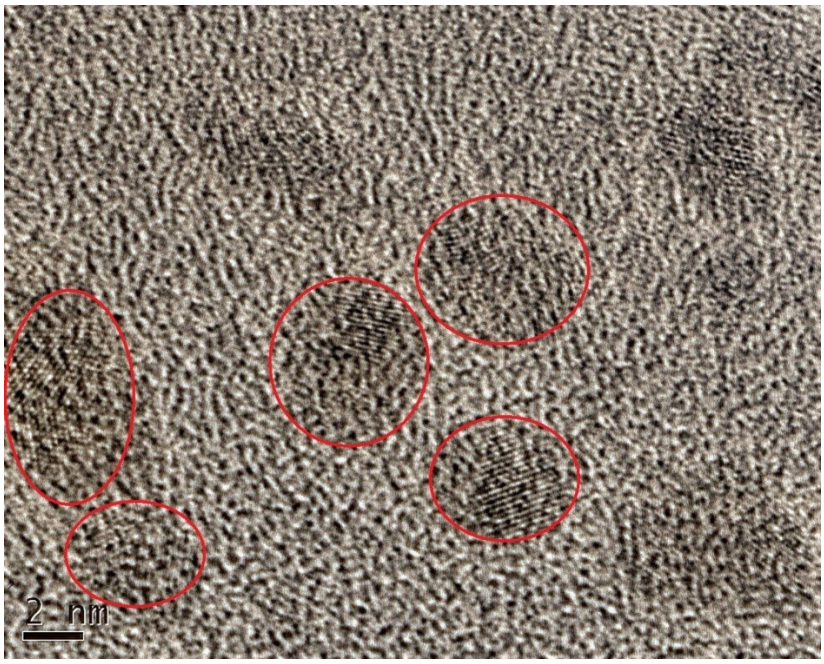

Fig. S8: HRTEM image of CG-MW with few marked particles.

Device Characterization

The Bode plot was derived from the impedance data. The electron lifetime was estimated by the following formula.

$$\tau_n = {}^{1}\!/_{2\pi f_{max}} \qquad \text{(I)}$$

Where 'τ_n' denotes the electron lifetime and 'f_{max}' denotes the peak frequency obtained in the low frequency region which caters to the charge transfer process happening at the working electrode and electrolyte interface.

The obtained J-V characteristics of CS2 taken instantly and after 100 min of illuminations under 1 sun condition is shown in Fig. S9. The device shows an almost perfect FF of ~85.60% with a V_{oc} of 0.5 V and a rather poor photocurrent of 20 μA.cm^{-2}. There is only a minor improvement in the photocurrent after 100 min of illumination which could be attributed to the junction formation of the device. In the case of CS3, the generated V_{oc} is also 0.5 V but there is a marked improvement in current (~ 65 μA cm^{-2}). Although after 100 min of irradiation, only a slight enhancement in potential is observed with almost similar generated current (Fig. S7a). Hence comparing CS2 and CS3, it seems that after 100 min of exposure, CS2 gains photocurrent while CS3 gains

photovoltage. Thus, upon combining the two sensitizers in one device, i.e., CS1, enhancement in both photocurrent and photovoltage is observed with prolonged illumination, thereby displaying synergistic interaction.

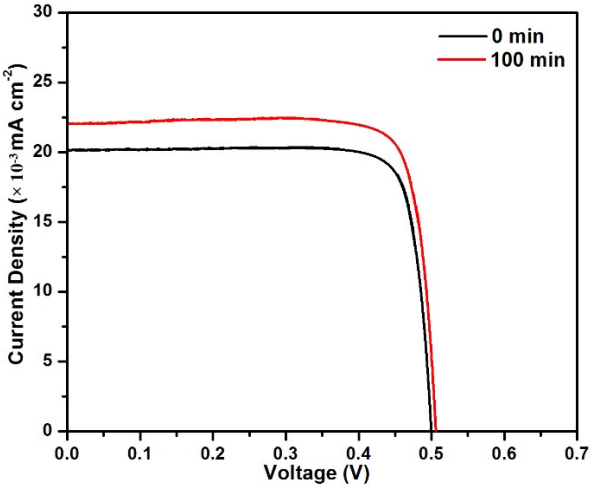

Fig. S9: J-V characteristics of CS2 under 1 sun condition.

Alternatively, CS3 was also irradiated with an LED lamp delivering 40 mW cm^{-2} input intensity for the same time period (Fig. S7b). Firstly, the generated photocurrent was quite poor (~ 8.1 $\mu A.cm^{-2}$) and secondly, it reduced by 1.4 $\mu A.cm^{-2}$ after 100 min of illumination with reduction in potential too. The poor device behavior of CS3 under white light LED is expected since it does not meet the N719 dye's requirement.

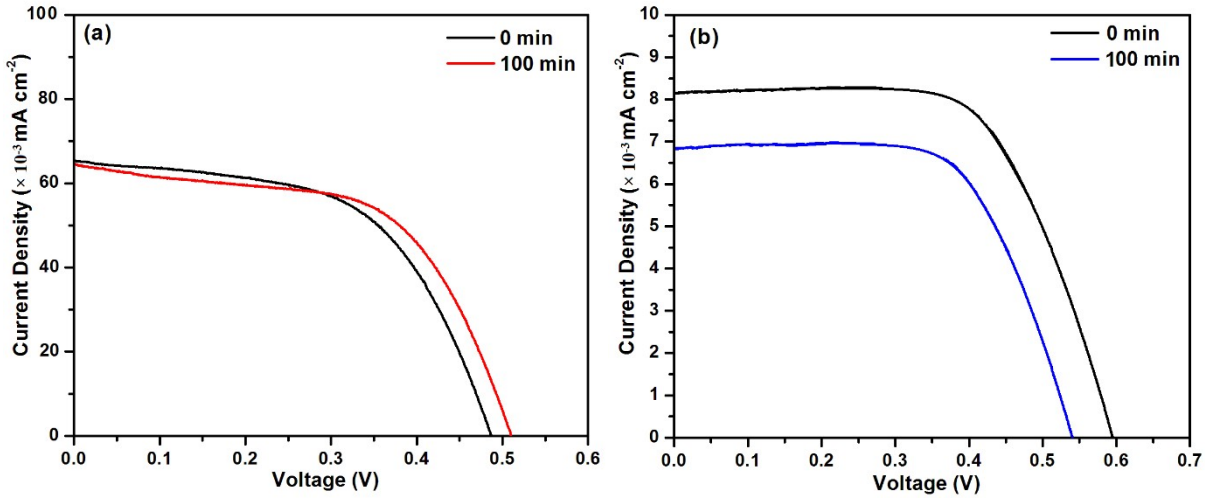

Fig. S10: J-V parameters of CS3 under (a) 1 sun illumination from xenon lamp and (b) 40 mW cm^{-2} illumination from LED lamp.

The performance of CS3 was also evaluated under room ambient condition wherein the input power was approximately 30 lux only. A sharp decline in current was observed for initial ~ 300 s following which the current gradually rose (Fig. S8). The light intensity across the device was merely 30 lux and the RT was ~ 30 °C. The rise in current under such dim lighting conditions clearly indicate the absorption of surrounding IR radiation. Owing to the weak energy of IR radiations and the dim lighting it took some time for the device to start converting the available energy into current. After ~ 6000 s the device was able to surpass its initial current value.

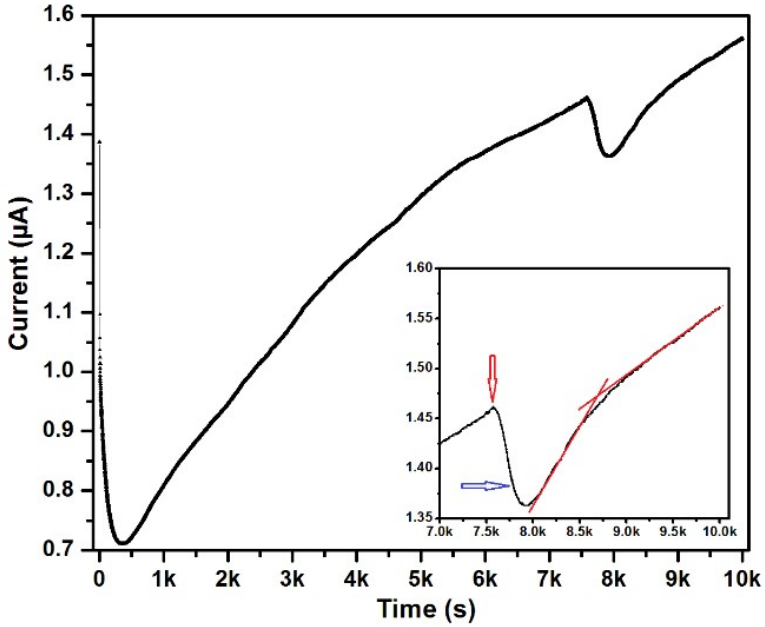

Fig. S11: I vs T measurement under room ambient lighting (~ 30 lux). (Inset) Expanded region when AC was turned ON. Red arrow marks AC ON and blue arrow marks AC OFF. The red lines indicate the change in slope.

To further assess the influence of IR radiations, at ~ 7500 s the AC was turned ON at 27 °C. Within seconds the air gradient around the device changed owing to the flow of cool breeze, which resulted in a sharp dip in the current (inset Fig. S8, red arrow). If the device was generating current only due to the room ambient light, no change would have occurred in the characteristics. The AC was turned OFF after about few hundred seconds, which again led to a gradual switching of the current path (blue arrow). At this point the surrounding air was still comparatively cooler, thus limiting the availability of IR radiations. After ~ 500 s when the availability of IR energy around

the device increased, a change in slope of the generated current is observed. This measurement essentially displays the device's operation capability even under dim light while affirming the its capability in utilizing the surrounding IR energy to generate micron order power.

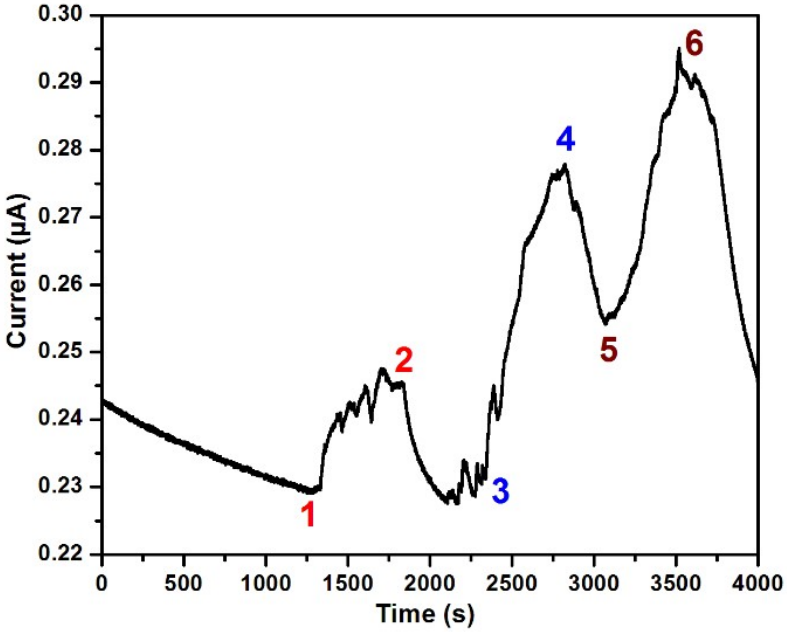

Fig. S12: CS2 subjected to time dependent current measurement at different conditions for assessing the impact of IR radiations. The numbers indicate the following: (1-2) Human hand brought close to the device with slight to-and-fro movement. (2-3) Human hand removed. (3-4) Soldering gun plugged-in for 5 min brought closer to device (1 cm away). (4-5) Soldering gun removed. (5-6) One side soldering gun and another side human hand. (6) Soldering gun and human hand removed. The experiment clearly establishes the sensitivity of device to nearby IR radiations, thereby doubling up as an IR sensor also.

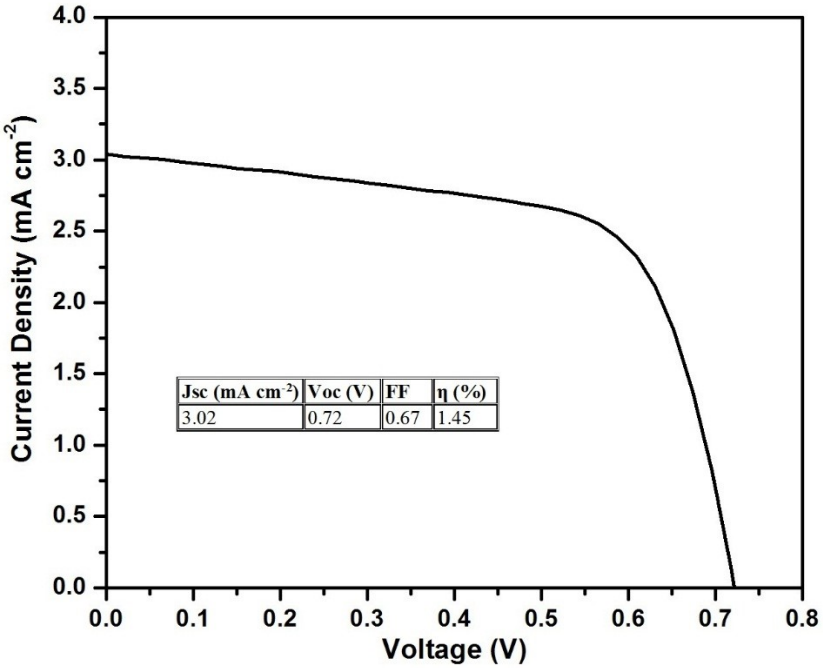

Fig. S13: The J-V characteristics of CS1.5 under simulated 1 sun illumination

References

[a] Yang, J.H., Bark, C.W., Kim, K.H. and Choi, H.W., 2014. Characteristics of the dye-sensitized solar cells using TiO_2 nanotubes treated with $TiCl_4$. Materials, 7(5), pp.3522-3532.

[b] Vaghasiya, J.V., Sonigara, K.K., Prasad, J., Beuvier, T., Gibaud, A. and Soni, S.S., 2017. Role of a phenothiazine/phenoxazine donor in solid ionic conductors for efficient solid state dye sensitized solar cells. Journal of Materials Chemistry A, 5(11), pp.5373-5382.

[c] Van Dam, B., Nie, H., Ju, B., Marino, E., Paulusse, J.M., Schall, P., Li, M. and Dohnalová, K., 2017. Excitation-dependent photoluminescence from single-carbon dots. Small, 13(48), p.1702098.

[d] Zhuo, Y., Miao, H., Zhong, D., Zhu, S. and Yang, X., 2015. One-step synthesis of high quantum-yield and excitation-independent emission carbon dots for cell imaging. Materials Letters, 139, pp.197-200.

[e] Fernandez-Jaramillo, A.A., Duarte-Galvan, C., Contreras-Medina, L.M., Torres-Pacheco, I., de J. Romero-Troncoso, R., Guevara-Gonzalez, R.G. and Millan-Almaraz, J.R., 2012. Instrumentation in developing chlorophyll fluorescence biosensing: A review. Sensors, 12(9), pp.11853-11869.